The Compact Muon Solenoid Experiment

Conference Report
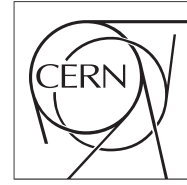
Test beam characterization of irradiated 3D pixel sensors

Andrea Garcia Alonso, Esteban Curras, Jordi Duarte-Campderros, Marcos Fernandez, Gervasio Gomez, Javier Gonzalez, Esther Silva, Ivan Vila, Richard Jaramillo, Marco Meschini, Rudy Ceccarelli, Mauro Dinardo, Simone Gennai, Luigi Moroni, Davide Zuolo, Natale Demaria, Ennio Monteil, Luigi Gaioni, Alberto Messineo, Gian-Franco Dalla Beta, Roberto Menicino, Maurizio Boscardin, Salvador Hidalgo, Angel Merlos, Giuliano Pellegrini, David Quirion, Maria Manna

Abstract

Due to the large expected instantaneous luminosity, the future HL-LHC upgrade sets strong requirements on the radiation hardness of the CMS detector Inner Tracker. Sensors based on 3D pixel technology, with its superior radiation tolerance, comply with these extreme conditions. A full study and characterization of pixelated 3D sensors fabricated by FBK is presented here. The sensors were bump-bonded to RD53A readout chips and measured at several CERN SPS test beams. Results on charge collection and efficiency, for both irradiated and non-irradiated samples, are presented. Two main studies are described: in the first the behaviour of the sensor is qualified as a function of irradiation, while kept under identical conditions; in the second the response is measured under typical operating conditions.

Presented at *iWoRiD 2019 21st International Workshop on Radiation Imaging Detectors*

Test beam characterization of irradiated 3D pixel sensors

A. García Alonso,[a,1] **E. Currás,**[a] **J. Duarte-Campderrós,**[a] **M. Fernandez,**[a] **G. Gomez,**[a]
J. Gonzalez,[a] **E. Silva,**[a] **I. Vila,**[a] **R. Jaramillo,**[a] **M. Meschini,**[b] **R. Ceccarelli,**[b] **M. Dinardo,**[c,d]
S. Gennai,[c,d] **L. Moroni,**[c,d] **D. Zuolo,**[c,d] **N. Demaria,**[e] **E. Monteil,**[e] **L. Gaioni,**[f,g] **A. Messineo,**[h]
G.-F. Dalla Beta,[i,j] **R. Menicino,**[i,j] **M. Boscardin,**[k] **S. Hidalgo,**[l] **Á. Merlos,**[l] **G. Pellegrini,**[l]
D. Quirion[l] **and M. Manna**[l] **on behalf of the CMS collaboration**

[a]*Instituto de Física de Cantabria (Universidad de Cantabria/CSIC),*
 Av. de los Castros s/n, Santander 39005, Spain

[b]*INFN, Sezione di Firenze,*
 Via Giovanni Sansone, 1, Sesto Fiorentino 50019, Firenze, Italy

[c]*INFN, Sezione di Milano-Bicocca, Dipartimento di Fisica G. Occhialini,*
 Università degli Studi di Milano-Bicocca, Edificio U2, Piazza della Scienza, 3, Milano 20126, Italy

[d]*University of Milano Bicocca,*
 Piazza dell'Ateneo Nuovo, 1, Milano 20126, Italy

[e]*INFN, Sezione di Torino,*
 Via Pietro Giuria, 1, Torino 10125, Italy

[f]*INFN, Sezione di Pavia,*
 Via Agostino Bassi, 6, Pavia 27100, Italy

[g]*Università degli studi di Bergamo,*
 Via Salvecchio, 19, Bergamo 24129, Italy

[h]*INFN, Sezione di Pisa and Università di Pisa,*
 Largo Bruno Fibonacci, 2, Pisa 56127, Italy

[i]*Università degli Studi di Trento,*
 Via Calepina, 14, Trento 38122, Italy

[j]*INFN, Sezione di Padova, Gruppo Collegato di Trento,*
 Via Sommarive, 14, Povo 38123, Trento, Italy

[k]*FBK-Fondazione Bruno Kessler,*
 Via Sommarive, 18, Povo 38123, Trento, Italy

[l]*Centro Nacional de Microelectrónica, IMB-CNM (CSIC), Campus UAB,*
 Carrer dels Tillers, Cerdanyola del Vallès 08193, Barcelona, Spain

 E-mail: agarciaa@cern.ch

---

[1]Corresponding author.

ABSTRACT: Due to the large expected instantaneous luminosity, the future HL-LHC upgrade sets strong requirements on the radiation hardness of the CMS detector Inner Tracker. Sensors based on 3D pixel technology, with its superior radiation tolerance, comply with these extreme conditions. A full study and characterization of pixelated 3D sensors fabricated by FBK is presented here. The sensors were bump-bonded to RD53A readout chips and measured at several CERN SPS test beams. Results on charge collection and efficiency, for both non-irradiated and irradiated up to $10^{16}\,\mathrm{n_{eq}/cm^2}$ samples, are presented. Two main studies are described: in the first the behaviour of the sensor is qualified as a function of irradiation, while kept under identical conditions; in the second the response is measured under typical operating conditions.

Contents

1 CMS Inner Tracker upgrade

An upgrade of the Large Hadron Collider (LHC) [1] is planned during the next long shutdown, turning it into the High Luminosity LHC or HL-LHC. Its instantaneous luminosity will increase to a peak value of 7.5×10^{34} cm^{-2} s^{-1}, roughly 4 times more than the running conditions in 2018, and reaching an integrated luminosity of 250 fb^{-1}/year [2]. These new conditions will enable the LHC experiments to enlarge their data sample by one order of magnitude. There will be a high track density, with up to 200 proton-proton interactions per bunch crossing at an interval of 25 ns.

To cope with these new conditions, the LHC experiments, including the Compact Muon Solenoid (CMS) detector [2], will be upgraded. In particular, the CMS Inner Tracker will be exposed to extreme fluences, setting a new challenge on the radiation tolerance of its sensors. Silicon sensors with active thicknesses between 100 and 150 μm are being considered. When segmented into 25×100 or 50×50 μm^2 pixels (narrower pitches than the present 100×150 μm^2 pixel detector) they provide a better transverse and longitudinal impact parameter resolution. The innermost pixel layer of the CMS detector will face fluences up to 2.3×10^{16} n$_{eq}$/cm^2. Therefore, sensors in this layer must be able to resist at least half of this value, expected when a technical stop and replacement is scheduled. To establish the best technology, able to suit all these requirements, two sensor technologies, planar and 3D, are under consideration.

2 3D pixel sensors for the Inner Tracker

This study focuses on 3D technology, which has been demonstrated to be able to work under such extreme conditions [3]. Its main characteristic is the arrangement of electrodes as columns perpendicular to the sensor surface (figure 1).

In this way, sensor thickness and distance between electrodes become independent, contrary to what happens in planar sensors, as shown in figure 1. Therefore, the full depletion bias voltage required in 3D technology is notably lower, resulting in lower thermal dissipation and avoiding potential sparking problems which can arise when operating at very high bias voltages. Moreover, the impact of charge carrier trapping is reduced, which, at large fluences, is a limiting factor for planar sensors.

The characterization of pixelated FBK[1] 3D sensors at different fluences, voltages and temperatures, has been carried out in several test beams. These sensors, whose transversal cut is shown

---

[1]Fondazione Bruno Kessler.
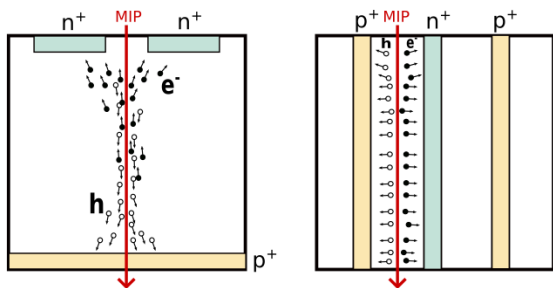
Figure 1. Planar (left) and 3D (right) sensor transversal cuts showing the collection paths towards the electrodes of electron hole pairs generated by an ionising particle [4].
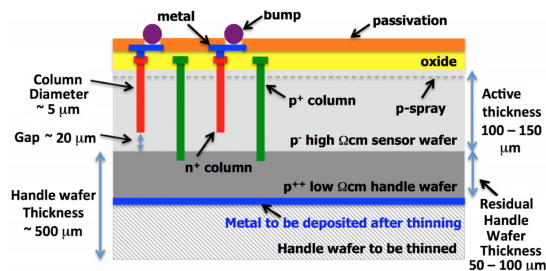
Figure 2. FBK 3D sensor transversal cut.

in figure 2, are fabricated in n-in-p single-sided technology on Si-Si wafers. The n-columns, where electrons are collected, are represented in the figure as red columns, while p-columns or ohmic contacts are in green. The electric field goes from n-type to p-type columns. The n-type columns are bump-bonded to the readout electronics to extract the signal.
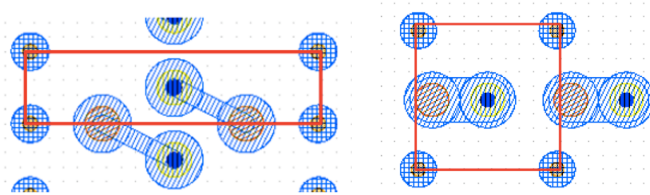
Figure 3. Pixel cell layouts of 3D sensors: $25{\times}100\,\mu m^2$ on the left and $50{\times}50\,\mu m^2$ on the right. The cell is represented here by the red shape, with the ohmic contacts at its corners and the pn junction column at the center, connected to the bump-pad.

In particular, we have obtained results from non-irradiated and irradiated 3D sensors in $25{\times}100\,\mu m^2$ (with one collecting electrode per cell) and $50{\times}50\,\mu m^2$ geometries, illustrated in figure 3. Their active thickness is 130 µm and the total thickness is 200 µm. They have no biasing structure and were bump-bonded to the RD53 collaboration pixel readout ASIC: the RD53A ROC [5]. The modules were mounted on specialized single-chip cards.[2] Data were collected from the RD53A ROC using the linear and synchronous front-ends. Results using the linear front-end are presented here.

3   Irradiation and test beam campaigns

The sensor characterization was performed in several test beams in the North Area of the CERN Super Proton Synchrotron (SPS), at the Prevessin site. A picture of the setup is shown in figure 4.

The proton beam energy was 120 GeV. For track reconstruction, an AIDA beam telescope consisting of six MIMOSA planes [8] was used. A time reference sensor was placed just after

---

[2]For more information about RICE and Bonn Single Chip Cards see ref. [6] and [7].

Figure 4. Test beam setup at the North Area of CERN SPS. Here two sensors are placed between the telescope planes.

the fourth telescope plane. The DUTs (Devices Under Test), controlled with BDAQ systems [9], were placed in the middle of the telescope. When testing the irradiated sensors, they were inside a cooling box (with humidity and temperature sensors) cooling down to $-30°$C.

The target fluence for these sensors is 10^{16} n_{eq}/cm^2 (1 MeV), which is roughly half of the total fluence expected inside CMS Layer 1, at a distance of 3 cm from the interaction point. In figure 5 the estimated neutron equivalent fluence is shown as a function of the column and row (col, row) index of the RD53A readout chip. The linear front-end is delimited by the large red rectangle. The irradiation took place in the PS-IRRAD Facility [10], with protons of 24 GeV/c momentum. Since the irradiation was not homogeneous, the linear front-end is divided in six regions of different average fluence. This way it is possible to compare the sensor response in exactly the same conditions but different fluences, studying the effects due to sensor damage alone.

4   Test beam results

In figure 5, the linear front-end has been divided into six rectangular areas, where a preliminary estimation of the average fluence in each is shown. Taking into account that these estimations are averaged values, we can be confident that in some zones of the middle and bottom right regions the target fluence has been reached.

In order to study these differences, as shown in figure 6, three areas of the linear front-end have been defined and named as 'Low', 'Medium' and 'High' fluence regions, with estimated values of 4×10^{15} n_{eq}/cm^2, 8.5×10^{15} n_{eq}/cm^2 and 10^{16} n_{eq}/cm^2, respectively.

When applying an unusually low bias voltage, the sensor is only depleted in the regions close to the pn junctions, and this provides us with a method to study the effects of irradiation. Figure 7 shows cell maps for the efficiency and charge collection of the 25×100 µm^2 sensor, for the three fluence regions, when a bias voltage of only 44 V is applied. A cell map is the superposition of all pixels inside a given fluence region into one single pixel cell. In this figure, the pn junction is located at position (50, 12.5) and the closest four ohmic contacts are on the corners of the cell map. The sensor response obtained here, in figure 7, is the worst possible due to the small depletion region (as a consequence of the low bias voltage), perpendicular particle incidence and high irradiation.
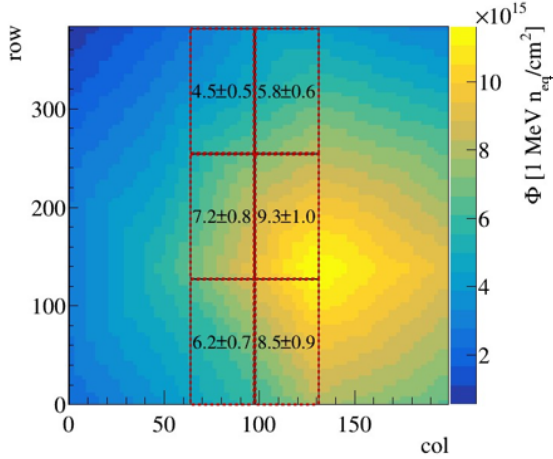
Figure 5. Neutron equivalent fluence as a function of pixel row and column number. The six regions cover the linear front-end. The average fluence estimation in each region is quoted, in n_{eq}/cm^2.
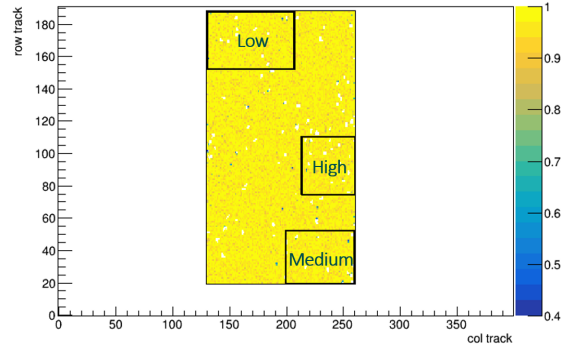
Figure 6. Efficiency map of the linear front-end, as a function of pixel row and column number, where the three fluence areas under study are marked. Only the part of the pixel matrix connected to the linear front-end was read out.

However, these conditions make possible to study the damage due to the irradiation. Later on, results for standard operation conditions will show the required sensor response.

In the efficiency maps (figure 7a) the effect of irradiation on the sensor is clearly visible. The sensor region with the lowest fluence shows the highest efficiency, with a value of 84%. As fluence is increased, the efficiency drops to 44% in the medium fluence region, and 38% in the high fluence region.

When increasing the fluence, the column structure (introduced in figure 3) also becomes clearer in the cell maps, as the homogeneous response of the sensor is lost. This behaviour is quantitatively observable in the projections over the column dimension. At a low fluence, the efficiency reaches 100% close to the pn junctions and as fluence increases it drops to around 20% at the ohmic contacts, and 90% at the pn junctions. Behaviour differences between the two kinds of columns are clearly visible in the medium and high fluence regions.

In terms of charge collection, there is a growth at the pn junctions as the sensor is irradiated. Charge collection is measured in Time Over Threshold (ToT) units, where 1 ToT represents around 1200 electrons. As indicated by the projections in figure 7b, charge collection at the pn junctions increases from 7.5 ToT in the low fluence region to 8.5 ToT in the high fluence region. This happens mainly because efficiency is biasing the charge towards higher values. Consequently, the main contributors to charge are the pn junctions, due to their better efficiency, and they contribute with greater values of charge since they are the areas which collect the most. Ohmic contacts collect less charge and their efficiency is lower, so their small contribution to charge remains out of the selection. Moreover, some multiplication effects could also be taking place.

The efficiency and charge collection shown in figure 8 were measured on fully depleted $25{\times}100\,\mu m^2$ sensors. Results before irradiation are obtained with a bias of 5 V (full depletion is quickly achieved in an unirradiated sensor), while irradiated sensors were biased at 125 V. The sensors were operated at normal beam incidence and $-36°C$ (except for the non irradiated sensor,
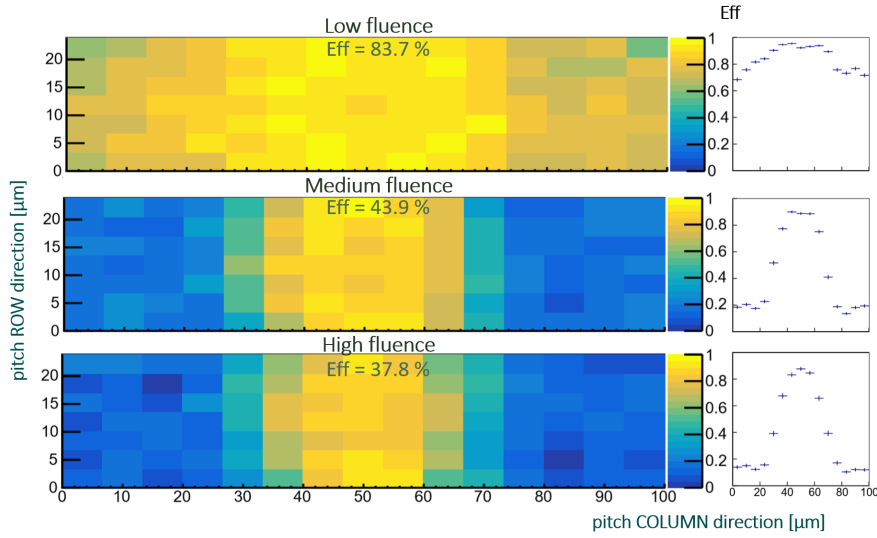
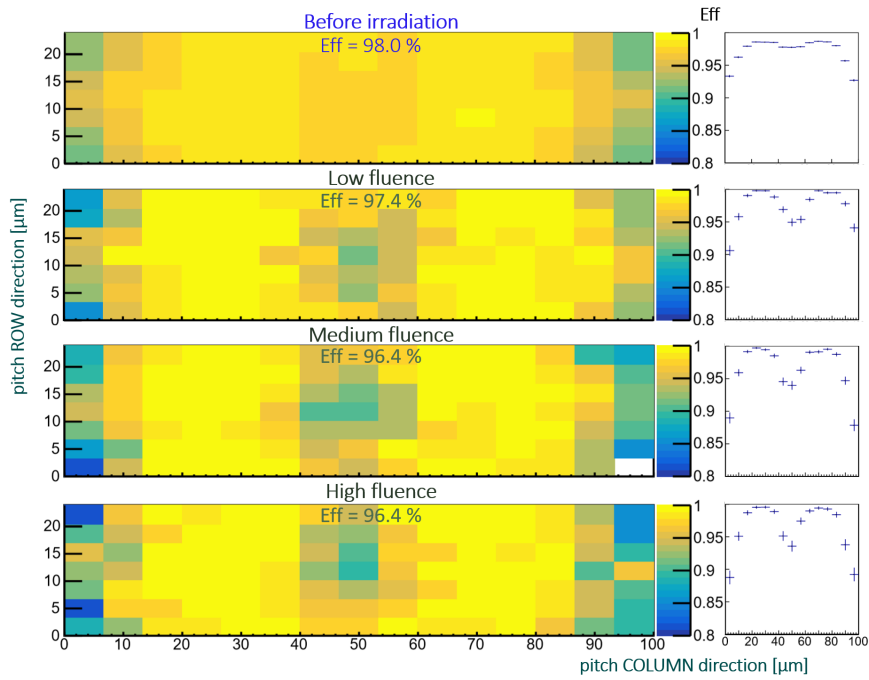**(a)** Efficiency pixel cell maps in the three different fluence regions.
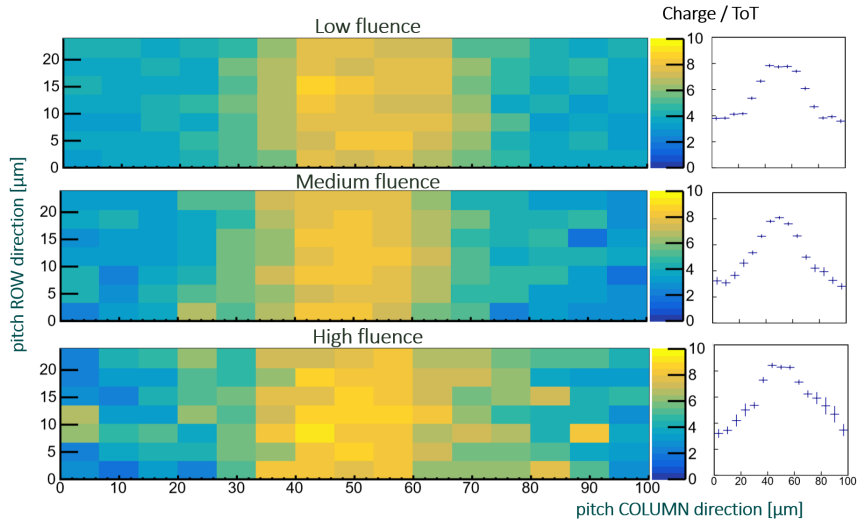
(b) Collected charge pixel cell maps in the three fluence regions. $1\,\mathrm{ToT} \approx 1200\,\mathrm{e}^-$.

Figure 7. Efficiency and collected charge when applying a low bias voltage of 44 V in a $25{\times}100\,\mu\mathrm{m}^2$ 3D sensor. Single pixel cell maps are shown on the left and their profiles over the column direction on the right.

which was measured at room temperature). Before irradiation, the global efficiency is 98%, while once irradiated the efficiency is still measured to be above 96%. As shown in figure 8a, before irradiation, the efficiency is more homogeneous along the pixel area, and the drop from the pn junctions to the ohmic contacts is just a 6%, while when irradiated this increases to around 10% (low fluence) or 12% (high fluence). In general terms, the efficiency is largely unaffected by radiation damage up to $10^{16}\,\mathrm{n_{eq}/cm^2}$.

The charge collection as a function of the pixel position is shown for the four neutron equivalent fluences in figure 8b. While increasing the fluence, there is a drop at the ohmic contacts, due to lower electric field and stronger trapping. At the pn junctions, a slight drop can be noticed, compared to the areas close to them, which is due to a geometrical issue: the sensor is fully depleted here but
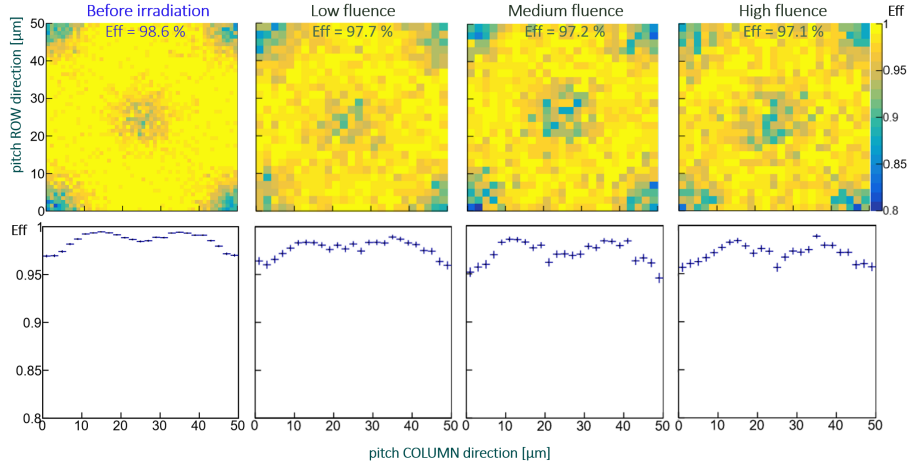
(a) Efficiency for the non-irradiated sensor and for the three different fluence regions of the irradiated sensor.
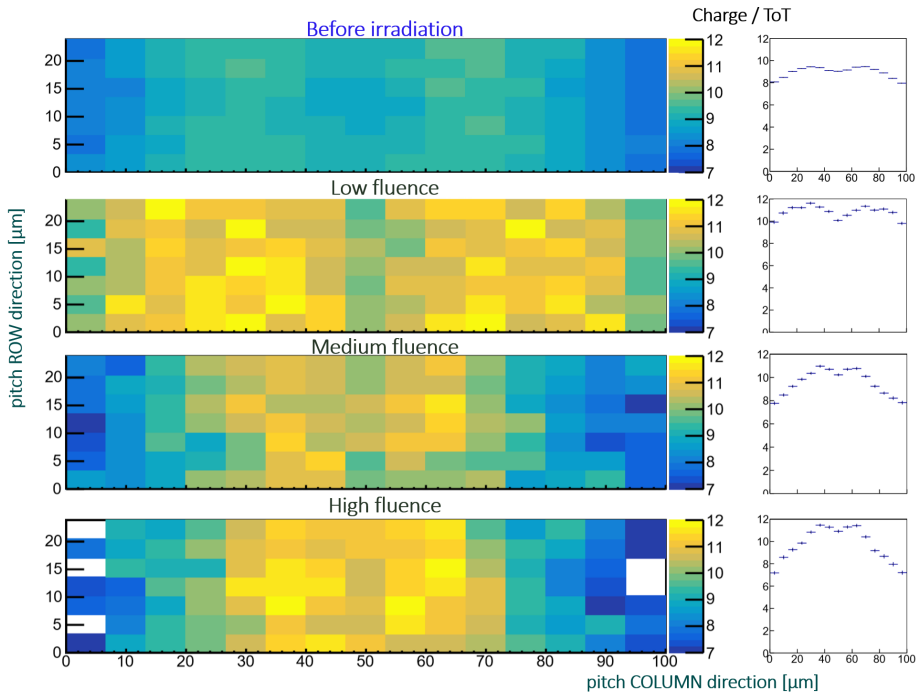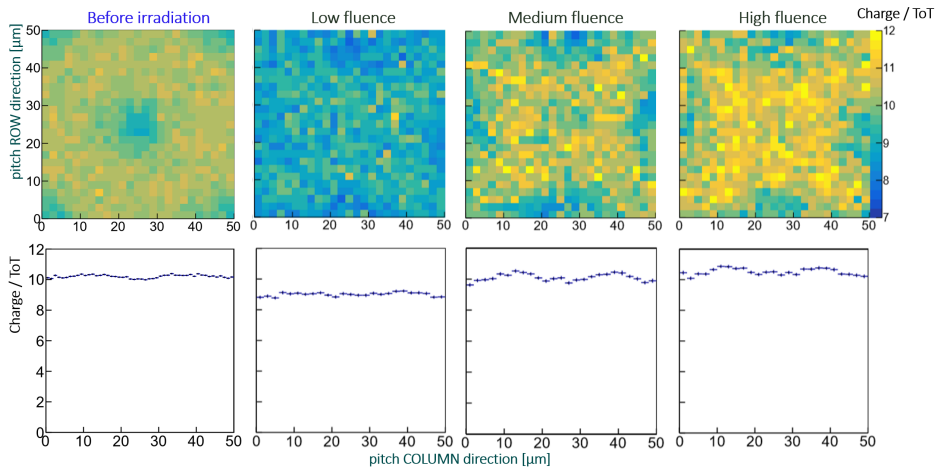

(b) Charge collection for the non-irradiated sensor and the irradiated sensor (separated in the three fluence regions). A ToT unit corresponds to approximately $1200\,e^-$ charges.

Figure 8. Efficiency and charge collection pixel cell maps when applying a bias voltage of $5\,V$ (to the non-irradiated) and $125\,V$ (to the irradiated) $25{\times}100\,\mu m^2$ 3D sensors. Single pixel cell maps are shown (left) and their profiles over the column direction (right).

(a) Efficiency pixel cell maps and profiles for the non-irradiated sensor and the three fluence regions of the irradiated one.

(b) Collected charge pixel cell maps and profiles for the non-irradiated sensor and the three fluence regions of the irradiated sensor (1 ToT $\approx 1200\,e^-$).

Figure 9. Efficiency and collected charge when applying 15 V (to the non-irradiated) and 151 V (to the irradiated) 50×50 μm² 3D sensors. In each case, single pixel cell maps are displayed on the top, and their profiles over the column direction on the bottom.

the particles impinge at normal incidence, which means that the column itself reduces the charge. Finally, at the points of high efficiency, the electric field gets more intense while increasing the fluence, generating a higher charge collection, which might be a sign of charge multiplication.

In the case of the 50×50 μm² geometry the conclusions are similar. For this geometry, the results from the sensor before irradiation were taken at room temperature, with an applied bias voltage of 15 V. The measured global efficiency is over 98%. For the irradiated sensor, during the test beam campaign, the applied bias voltage was 141 V, and the temperature −36°C inside the cooling box. After irradiation, the global efficiency was measured to be above 97%. Regarding the global efficiency per fluence region (figure 9), this magnitude remains constant in every case, so here again we can establish that the efficiency for these 3D sensors can also be maintained even

after irradiation up to 10^{16} n_{eq}/cm^2. Similarly, when increasing the fluence, efficiency losses about 4% towards the ohmic contacts become present. Anyhow this is a negligible variation.

In terms of charge collection, figure 9b, a new effect is observed: as the sensor is progressively damaged under irradiation, the charge collection mainly increases along the diagonals connecting pn junction and ohmic contacts in the single pixel cell map. This larger charge collection with increasing fluence hints towards increasing electric fields following this path, generating some charge multiplication along the diagonals (see the profiles from the irradiated sensor in figure 9b).

5 Conclusions and outlook

The results demonstrate that 3D sensors represent an appropriate option for the CMS Inner Tracker at the HL-LHC. As presented, radiation damage up to 10^{16} n_{eq}/cm^2 does not significantly affect sensor performance. Before and after irradiation, the sensors present a high efficiency, always above 96% in operation conditions, and good charge collection.

The non-homogeneous irradiation of the sensor provided the opportunity to study the same sensor under identical conditions as a function of fluence only. Differences in charge collection at the pn junctions and ohmic contacts, the effects due to depletion changes when increasing the fluence, and reductions in charge collection and efficiency with sensor damage were all observed.

When studying the sensor under standard operating conditions, achieving full depletion, at normal incidence, multiplication effects are observed for fluences of 4×10^{15} n_{eq}/cm^2, 8.5×10^{15} n_{eq}/cm^2 and 10^{16} n_{eq}/cm^2 and efficiencies around 100% are obtained in the inter-columnar region. Efficiency is maintained after irradiation, establishing that 3D sensor response is not degraded with fluences up to 10^{16} n_{eq}/cm^2. And all this for both pixel geometries, 25×100 and 50×50 μm^2.

References

[1] L. Evans and P. Bryant, *LHC Machine*, 2008 *JINST* **3** S08001.

[2] CMS collaboration, *The Phase-2 Upgrade of the CMS Tracker*, CERN-LHCC-2017-009 (2017).

[3] E. Currás et al., *Study of small-cell* 3D *silicon pixel detectors for the high luminosity LHC*, *Nucl. Instrum. Meth.* **A 931** (2019) 127 [arXiv:1806.01435].

[4] J. Duarte-Campderros et al., *Results on Proton-Irradiated* 3D *Pixel Sensors Interconnected to RD53A Readout ASIC*, *Nucl. Instrum. Meth.* **A 944** (2019) 162625.

[5] RD53 collaboration, *The RD53A Integrated Circuit*, CERN-RD53-PUB-17-001 (2017).

[6] T. Nussbaum, K. Ecklund and A. Kumar, *Irradiation Adapter for single chip RD53A+sensor modules*, talk given at *RD53A testing*, 4 September 2018, CERN, Geneva 23, Switzerland and online pdf version at https://indico.cern.ch/event/754920/contributions/3128413/attachments/17104/2757181/RiceSCC.pdf.

[7] M. Daas, T. Hemperek, J. Janssen, H. Krüger, D.-L. Pohl and M. Vogt, *Characterization and verification environment for the 65 nm pixel readout chip RD53A*, in proceedings of the *Topical Workshop on Electronics for Particle Physics (TWEPP-17)*, Santa Cruz, California, 11–14 September 2017 and online pdf version at https://indico.cern.ch/event/608587/contributions/2614134/attachments/1523734/2381558/RD53A-testsystem_Vogt_Bonn_TWEPP17.pdf.

[8] CERN collaboration, *MIMOSA Telescope*, (2020) https://twiki.cern.ch/twiki/bin/view/MimosaTelescope/.

[9] M. Daas and M. Vogt, *BDAQ53 Readout hardware*, (2020) https://gitlab.cern.ch/silab/bdaq53/wikis/Hardware/Readout-Hardware.

[10] B. Gkotse, M. Glaser, M. Moll and F. Ravotti, *IRRAD: The New* 24 *GeV/c Proton Irradiation Facility at CERN*, in proceedings of the *12th International Topical Meeting on Nuclear Applications of Accelerators (AccApp 2015)*, Washington, D.C., U.S.A., 10–13 November 2015 and online at http://accapp15.org/wp-content/data/62105-ans-1.3388085/t006-1.3388638/f006-1.3388639/15627-1.3388652.html.